Available online at www.sciencedirect.com
SCIENCE DIRECT
ELSEVIER
Polymer 46 (2005) 9097–9112
polymer
www.elsevier.com/locate/polymer

Mechanical gradient interphase by interdiffusion and antiplasticisation effect—study of an epoxy/thermoplastic system

M. Munz[a,*], H. Sturm[a], W. Stark[b]

[a]*Federal Institute for Materials Research and Testing (BAM), Div. VI.2 'Mechanics of polymers and composites', Unter den Eichen 87, D-12205 Berlin, Germany*
[b]*BAM, Div. VI.1 'Durability of polymeric materials', Unter den Eichen 87, D-12205 Berlin, Germany*

Received 11 April 2005; received in revised form 16 June 2005; accepted 22 June 2005
Available online 24 August 2005

Abstract

A stoichiometric amine–epoxy formulation was cured in the presence of a thermoplastic, namely poly(vinylpyrrolidone) (PVP). The epoxy system consisted of the resin diglycidyl ether of bisphenol A (DGEBA) and the aromatic curing agent 4,4′-diaminodiphenylsulfone (DDS). As shown for this system in a former study by Oyama et al. [Oyama HT, Lesko JJ, Wightman JP. J Polym Sci B 1997;35:331–46. [36]], preferential absorption of amine molecules by PVP can occur. In the present study, the focus is on the variations of local elastic properties within the epoxy interphase adjacent to the PVP layer. The curing was performed close to the glass transition temperature, T_α, of the PVP film, namely at 170 °C. Variations of the local amine concentration were tracked using energy-dispersive analysis of X-rays (EDX), by taking benefit of the sulfur contained in DDS. Using temperature-dependent dynamic mechanical analysis (DMA), a series of epoxy reference samples of different amine–epoxy concentration ratios, r, was investigated in order to work out the relationship between r and the epoxy storage modulus at room temperature. In the excess-epoxy regime, $r<1$, the modulus is observed to increase with departure from the stoichiometric ratio, $r=1$. Considering the respective suppression of the β-transition, the observed characteristic can be explained by an antiplasticisation effect. Depth-sensing indentation (DSI) experiments across the epoxy/PVP interphase provided evidence for strong modulus variations. In consistency with the EDX and the DMA data, in the vicinity of the PVP layer the local epoxy modulus is increased. The total change of the epoxy Young's modulus is ~1.1 GPa. However, the total width of the modulus decay of ~175 μm is ~2.5 times larger than the one of the DDS concentration gradient. This finding is discussed in terms of additional spatial variations of the DGEBA concentration as well as long-range diffusion currents of DDS induced by the interdiffusion processes and their effect on the final network of crosslinks.

Keywords: Interdiffusion; Interphase/interface; Polymer

1. Introduction

Geometrically, an interface between two materials is the two-dimensional border separating them. However, owing to physical and chemical interactions at the location of the interface, in its vicinity there can exist a region, where a gradual transition from bulk properties of one material to those of the other one occurs. Such kind of region with non–zero volume is generally referred to as interphase (in the following denoted as IP). The IP width depends on the particular interfacial interaction mechanisms as well as on the nature of the bonded materials.

In the case of two incompatible, amorphous and thermoplastic polymers, the IP width is expected to be in the order of the radius of gyration of the macromolecules, that is in the range of 2–50 nm [1]. When dealing with a semi-crystalline polymer, however, interfacial interactions were observed to induce strongly modified crystalline morphologies, in particular transcrystalline ones, extended over tens of microns in the direction perpendicular to the interface [2,3]. In a similar manner, polymerisation or crosslinking reactions can be affected by the adjacent surface of the second material. In particular, when starting

* Corresponding author. Tel.: +49 30 8104 1623; fax: +49 30 8104 1627.
E-mail address: martin.munz@bam.de (M. Munz).

0032-3861/$ - see front matter © 2005 Elsevier Ltd. All rights reserved.
doi:10.1016/j.polymer.2005.06.098

from a low-viscosity mixture of a two-component system, long-range diffusional currents can occur. If there exists a thermodynamic driving force for the preferential adsorption of one of the components, this interface-induced segregation results in concentration gradients, which can translate into spatial variations of morphology and related properties of the cured system. A two-component reactive polymer system of particular practical relevance is epoxy resin mixed with a curing agent, e.g. a diamine. A large number of studies is available, focused onto interface effects of such thermosets filled with fibres [4–9], microscale particles [10–13], or nanoscale particles [14–17]. Another type of composite less frequently investigated is with a thermoplastic polymer. In addition to the fundamental interest, such kind of thermosetting–thermoplastic combination is of high practical relevance. In many applications, thermoplastic parts are coated with a thermosetting surface layer for decorative or protective purposes. Frequently, thermoplastic parts are connected via thermosetting adhesives. Furthermore, a thermoplastic can be used as a sizing agent for fibres to be embedded into an epoxy matrix [18,19]. Also toughened epoxy can be produced by blending it with a thermoplastic [20].

In contradiction to a solid filler, the thermoplastic component does not provide an impenetrable barrier, but rather may absorb low-molecular weight species of the reacting thermosetting system or even mix with the reactive polymer formulation. Thus, beyond the surface of the thermoplastic component also its bulk morphology as well as its mechanical and thermal properties are involved. Moreover, the absorbed molecular species affect the molecular dynamics of the thermodynamic host molecules. By this way, they alter the conditions for further interdiffusion, thus resulting in a concentration-dependent diffusion coefficient [21,22].

On the side of the epoxy, the spatial concentration variations induced by the interdiffusion processes are expected to affect the final chain network, including its topology and related parameters, such as crosslink density and packing density. According to the rubber elasticity theory, the crosslink density is given by the inverse of the average molecular weight between crosslinks, $1/M_c$. The packing density can be given by the strand density, i.e. the effective concentration of network chains per volume, $\nu=(\rho N_A)M_c$ (where ρ denotes the mass density and N_A Avogadro's number). These parameters are of major relevance for the final mechanical properties of the cured epoxy. For instance, the rubber modulus is proportional to the strand density ($G_r \propto \nu k_B T$) [23].

Thus, interphasial concentration gradients imply corresponding gradients of local mechanical properties, such as strain-to-failure or Young's modulus. The latter is a key parameter for the spatial distribution of mechanical stresses. Depending on the modulus profile, various interfacial stress distributions may occur. As shown by means of finite element simulations [24], step or peak stress gradients can occur within the IP. Initial cracks are likely to occur at the locations of peak stresses. On the opposite, property gradients may be generated which favour low interphasial stress levels rather than stress peaks. In general, such sort of materials exhibiting regions of well-aimed and continuous property variations are referred to as functionally graded materials (FGM) [25,26]. Similarly, graded morphologies were generated between epoxy and a miscible thermoplastic taking benefit of the mechanism of reaction-induced phase separation [27–29]. Beyond the mechanical properties, also chemical property variations across the IP can play a major role for the reliability of the composite, for instance concerning the environmental failure of adhesive joints [6,8,13,30].

Lack of knowledge of quantitative IP properties was identified by Lesko et al. as 'the Achilles heel of the field' [31]. Although the relevance of IP properties appears to be generally accepted, there exists only a limited number of investigations providing quantitative information on mechanical IPs, including parameters such as IP width, total modulus change across the IP, or radial stiffness profile [9,32–35]. Owing to the availability of advanced micro- and nano-indentation techniques, mapping of local stiffness has become possible with a high spatial resolution.

In the present study, the epoxy-sided IP of an epoxy/thermoplastic-IP was investigated with emphasis on mechanical property variations. The epoxy resin of type diglycidyl ether of bisphenol A (DGEBA) was cured using the aromatic diamine 4,4′-diaminodiphenylsulfone (DDS). Similarly to a study by Oyama et al. [36], the thermoplastic component was poly(vinylpyrrolidone) (PVP). PVP is an amorphous vinyl polymer having a pendant lactam ring. Owing to its carbonyl group, PVP is expected to establish hydrogen bond interactions with epoxy systems.

Using energy-dispersive analysis of X-rays (EDX), Oyama et al. observed IP concentration variations of the amine curing agent, indicating partial absorption of the amine by the PVP layer via interdiffusion processes. These take place during the curing of the epoxy in the presence of the thermoplastic [36]. By mixing the standard DGEBA with brominated DGEBA, in EDX the Br-signal allowed spatial epoxy concentration variations to be tracked. From the combined analysis of the N-, S-, and Br-signals, concentration profiles for PVP, DDS as well as DGEBA were deduced. The width of the concentration profiles was shown to increase with the temperature of the initial cure stage (130 and 170 °C) as well as with decreasing molecular weight of PVP. The initial stage of the two-step curing cycle (post-curing at 220 °C) was decisive for the interdiffusion processes [36,37]. Furthermore, Oyama et al. concluded that the diffusion front of DDS was located several microns closer to PVP than that of the epoxy [36].

On the contrary to the work by Oyama et al. in the present study the used epoxy resin was neat DGEBA rather than a mixture with brominated DGEBA. By that way, any additional effects potentially occurring due to the use of a

mixture of two different resins were avoided as well as related complications with the mechanical properties of the cured epoxy. In addition, the polarity of the brominated DGEBA may cause differences in the interfacial interactions [36]. Also a faster curing reaction was reported for systems with brominated DGEBA [36,38].

The paper is organised as follows: In Section 3, the results of the EDX measurements of spatial concentration variations are described. Section 4 is devoted to the temperature-dependent dynamic mechanical analysis (DMA) of a series of epoxy reference samples of well-defined amine concentration ratios. A relationship between the concentration ratio and the epoxy modulus measured at room temperature (RT) is derived and discussed in conjunction with the corresponding changes of the β-transition. In Section 5, the modulus profiles from the depth-sensing indentation (DSI) experiments (approach B) are presented and compared to the modulus profiles deduced via the EDX and DMA results (approach A). Finally, in Section 6 the results from both approaches are discussed in the light of possible effects other than the amine concentration gradient. The conclusions are given in Section 7.

2. Experimental

Polyvinylpyrrolidone (PVP) films were prepared using powder of PVP as supplied by Fluka. For the chemical structure of PVP see Fig. 1. The K-90 grade corresponds to a number average molecular weight $M_n \sim 360{,}000$ (viscosity average molecular weight $M_v = 1{,}100{,}000$) [39]. PVP was dissolved in a 1:1 mixture by volume of distilled water (grade pro analysis, by Merck) and methanole. About 5.5 g of PVP were dissolved in 40 ml of the water–methanole mixture. From this solution, films were cast in Teflon moulds. For purpose of drying, these films were stored for two weeks at RT and for another two weeks at 80 °C. In order to avoid stress-induced cracking of the films, the process of drying was kept slow by storing the moulds in covered containments with small openings only for ensuring limited gas exchange. The final thickness of the PVP films was in the range of 50–150 μm.

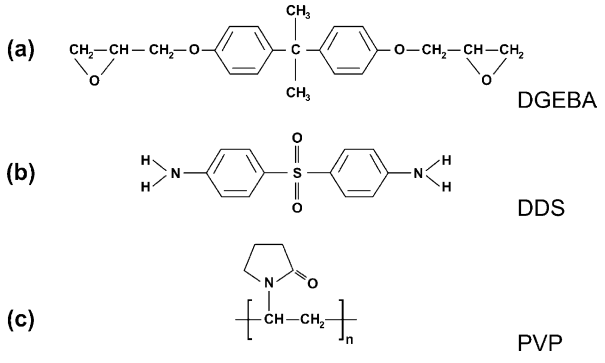

Fig. 1. Molecular structure formula of (a) the epoxy resin DGEBA, (b) the curing agent DDS, and (c) the thermoplastic PVP, respectively.

The epoxy resin used was of type diglycidyl ether of bisphenol A (DGEBA) with a condensation factor n of the higher molecular weight homolog close to zero, namely DER332 (by Dow Chemical, Stade, Germany). Accordingly to $n \sim 0$, the average epoxy equivalent weight, EEW, of DER332 (EEW ∼ 174 g/mol) is close to that of chemically pure DGEBA (EEW ∼ 170 g/mol) [40]. The diamine curing agent used was 4,4′-diamino-diphenylsulphone (DDS), the molecular weight of which is given by the manufacturer as 248.3 g/mol.

The DGEBA as well as the DDS molecule contain two ones of the respective chemical groups responsible for the curing reaction, namely the epoxy (oxirane) group and the primary amine group, respectively (Fig. 1). These reactive groups are situated at the ends of the molecules. Since one primary amine group is expected to react with two epoxy (oxirane) groups, $N_e = 2$ mol of DGEBA correspond to $N_a = 1$ mol of DDS. Thus, the amine–epoxy mixing ratio, r, can be defined as follows [41]:

$$r = \frac{N_a}{N_e}\frac{f_a}{f_e} \tag{1}$$

where f_a and f_e denote the chemical functionality of the amine and the epoxy molecules, respectively. The corresponding values for DDS and DGEBA are $f_a = 4$ and $f_e = 2$. Two different concentration regimes can be distinguished, namely the under-stoichiometric regime (excess epoxy) and the over-stoichiometric one (excess amine). These regimes are given by $r < 1$ and $r > 1$, respectively. The demarcation $r = 1$ denotes the stoichiometric case (equimolar ratio). For purpose of studying the relationship between stoichiometry and mechanical properties of the cured epoxy, samples of different concentration ratios were prepared, with r ranging from 0.6 to 2.0. Typically, the total mass of the mixture was ∼47 g.

For mixing and curing a temperature-controlled oil bath was employed (model TP-6 by Julabo Labortechnik, Seelbach, Germany). The mixture of epoxy resin and curing agent was contained in a 400 ml glass beaker, the lower half of which was immersed into the oil bath. For avoiding exposition to oxygen or humidity, the glass beaker was capped and rinsed with nitrogen. A glass-stirring rod was fed through a sealed opening in the lid. By this way, stirring was possible under controlled gas conditions and a precise and quick temperature control was provided by means of the oil bath. First, the liquid epoxy resin was added at 50 °C, heated up to 110 °C, and kept at this temperature for 60 min in order to reduce the water content possibly taken up by the epoxy resin during storage. Then, the appropriate amount of DDS powder was added and the temperature was increased up to 160 °C within 8 min. At this temperature, DDS dissolved very well in DER332 while the low-viscosity mixture was thoroughly stirred over 7 min. Afterwards, the

stack of Teflon moulds was immersed into the reactive mixture. Before immersing, the stack was stored at a temperature of ~110 °C for ~120 min as a final drying step for the PVP film (which was deposited into one of the moulds of the stack). As well as the heated storage of the epoxy resin, this was done under flow of nitrogen.

The diameter of the circular Teflon moulds was designed to fit gently into the glass beakers. Typically, a stack consisted of a base plate, one mould for casting an epoxy bar later to be used for DMA, one mould containing the PVP film, and a top plate. Upon immersion, the moulds were flooded with the liquid epoxy formulation. Both the top and the bottom side of the PVP film were covered, thus resulting in a sandwich-like sample with the PVP layer as the central one. The thickness of the epoxy layers was ~4 mm.

The temperature of isothermal epoxy curing was 170 °C. The ultimate glass transition temperature, $T_{\alpha\infty}$, of the fully cured DGEBA-DDS system is ~218 °C [42]. Thus, in order to circumvent vitrification and the resulting diffusion-control of reaction rate, a similar or higher curing temperature is required for achieving $T_{\alpha\infty}$. However, no such post-curing step was applied for avoiding oxidative effects taking place in PVP.

Owing to peroxide residues resulting from its production, oxidation may occur in PVP. Throughout a wide range of molecular weights the main temperature of oxidation was observed to be ~30 °C above T_α [43]. The oxidation of PVP comes along with a small loss of weight and some crosslinking, which can prevent complete dissolution. Furthermore, above ~200 °C degradation may be observed in blends of PVP and DGEBA, with PVP exhibiting a stabilising effect on DGEBA, but PVP being destabilised by DGEBA [44]. In our case, thermogravimetric analysis (TGA) applied to PVP-K90 under flow of nitrogen showed some loss of mass in a region of temperatures ranging from ~180 to ~290 °C. In comparison, for a PVP-K30 sample the corresponding onset temperature of mass loss was ~140 °C and the degree of mass loss was much more pronounced. The epoxy was cured in the presence of the PVP-K90 film. As deduced from differential scanning calorimetry (DSC) measurements of the PVP-K90 film before the final drying step, its centre T_α value was ~169 °C, with the onset at ~158 °C. As visible from the data presented by Tan and Challa [45], the extrapolated onset-T_α value of PVP-K90 at zero water content is ~175 °C and a decrease of T_α of ~9.8 °C/wt% of water content is observed in the low concentration range (<7.5 wt%). As applied to our PVP-K90 sample, this suggests that it contained ~1.7 wt% water before the final drying step at ~110 °C was undertaken.

With 170 °C, the isothermal curing temperature was close to the T_α of the PVP film. Considering the DGEBA-DDS system, the final degree of cure achievable at 170 °C is ~85% [41]. This degree is reached after ~120 min. After this period of time, the beaker was removed from the oil bath and cooled down to RT.

From the epoxy bar (thickness ~8 mm), a beam-shaped DMA sample of dimensions $60\times10\times0.6\ mm^3$ was prepared by polishing. Care was taken to keep the thickness variations across the DMA beams as low as possible. Using these beams, DMA measurements in torsional pendulum configuration (model ATM-3 by Myrenne Instruments, Roetgen, Germany) were performed in the temperature range from −180 to +270 °C. For each DMA beam, both a heating and a subsequent cooling temperature scan were passed through. The heating and cooling rates were ~±1.1 K/min, respectively. The torsional pendulum frequency was ~1 Hz.

Cross-sections of the epoxy/PVP/epoxy samples were prepared using an ultramicrotome (Ultracut UCT by Leica Mikrosysteme GmbH, Vienna, Austria). Microtoming was done at RT, using an 'Ultra30' type diamond knife (by Diatome, Biel, Switzerland).

Depth-sensing micro-indentation experiments (so-called compliance method) were performed by means of a commercial indenter set-up (model 'Triboscope' by Hysitron, Minneapolis, MN), combined with a home-built imaging system [46]. In the imaging mode, the sample was raster-scanned while the tip-sample force was kept constant by adjusting the tip height, thus following the sample topography. The indenter was of Berkovich type, i.e. a three-sided pyramid with an ideal projected area-to-depth function given by the square of the depth of contact [9,47,48]. The opening angle of the Berkovich indenter is 130.6° [48]. However, in general deviations from this simple relationship have to be taken into account, due to blunting of the apex of the tip. The particular area-to-depth function of the indenter to be used was determined by means of an epoxy sample, the Young's modulus value of which was ~3.08 GPa. The maximum load of the force-penetration curves was ~9.7 mN, resulting in a typical penetration depth of ~1.4 μm. Loading and unloading were done with a rate of 2 mN/s. In each loading sequence, between the loading and the unloading step, a hold period of 30 s was inserted in order to allow any creeping effects to take place before starting the unloading step. If not inserting a hold period it may happen that creeping is superimposed to the elastic displacements recovered during unloading. This effect can be readily observed by the occurrence of a round shape at the loading–unloading part of the force–displacement curve [49].

An XL30 type scanning electron microscope (by FEI/Philips, Eindhoven, The Netherlands) was employed for performing the energy-dispersive analysis of X-rays (EDX). The EDX detector was of the sapphire type with a super-ultrathin window (by EDAX, Mahwah, NJ). Typically, the acceleration voltage was 11.0 kV. For avoiding charging effects, the sample was coated with a thin film of Ti with a thickness of ~36 nm, as measured by means of a microbalance integrated into the PVD chamber (Auto 306 vacuum coater equipped with an EB3 electron beam set-up, by Edwards High Vacuum International, Crawley, UK). The

corresponding Ti Kα peak of the EDX spectrum was used as a reference signal. By calculating the ratio of the peak area to be studied to that of the Ti Kα peak at 4.51 keV, measurement-to-measurement variations originating from variations in electron beam tuning or sample tilt were taken into account. The S Kα peak at 2.31 keV was used for tracking local concentration variations of DDS across the PVP/epoxy IP. The borderlines of the PVP layer were identified by means of the N Kα signal at 0.39 keV which shows a step-like change across the PVP/epoxy interface. Due to limited resolution at low energies, the N Kα signal was overlapping to a low degree with the O Kα signal at 0.51 keV.

For purpose of simulating the EDX measurements on epoxy of different amine concentration ratios, the dedicated Monte Carlo simulation package CASINO, Version 2.42 (by Drouin et al., University of Sherbrooke, Que., Canada) was employed [50–52]. Hereby, the used effective section ionisation model was the one by Pouchou.

Data smoothing and fitting were achieved by means of the software TableCurve2D (by Systat Software Inc., Richmond, CA). For smoothing (Sections 3 and 5) as well as for calculation of a smoothed interpolation spline (Section 4), the algorithm by Savitzky and Golay was used.

3. Concentration mapping across the interphase

Starting from a stoichiometric and low-viscosity mixture of epoxy resin (DGEBA) and curing agent (DDS), the epoxy system was cured in the presence of the PVP film. Driven by the preferential interaction of either DGEBA or DDS with PVP, spatial variations of the concentration ratio, r, can occur. Since the viscosity of the epoxy–amine mixture is rising fast with the degree of reaction, these effects are most likely to happen in the early phase of the curing procedure. From the point of time, where gelation is reached and the viscosity diverges, however, any hitherto developed concentration gradients can be considered as frozen.

In order to detect such concentration variations, after curing cross-sectional surfaces of the epoxy/PVP/epoxy sandwich samples were prepared and investigated employing EDX. The orientation of the cross-sections was perpendicular to the epoxy/PVP interfaces. The Kα transition of the S contained in DDS provides a sufficient signal-to-noise ratio and can be used for tracking spatial variations of the DDS concentration. A corresponding S-map is given in (Fig. 2(c)), alongside with an N-map (Fig. 2(b)) and an SEM micrograph (Fig. 2(a)).

On PVP the intensity of the N-signal is increased and a rather abrupt intensity change is observed at the edges of the PVP cross-sectional area. Thus, from the N-map interfacial borderlines were deduced which are drawn into the images as white dashed lines. On the contrary to the N-map, the S-map exhibits the higher signal intensity on the outer epoxy regions. Furthermore, when approaching the

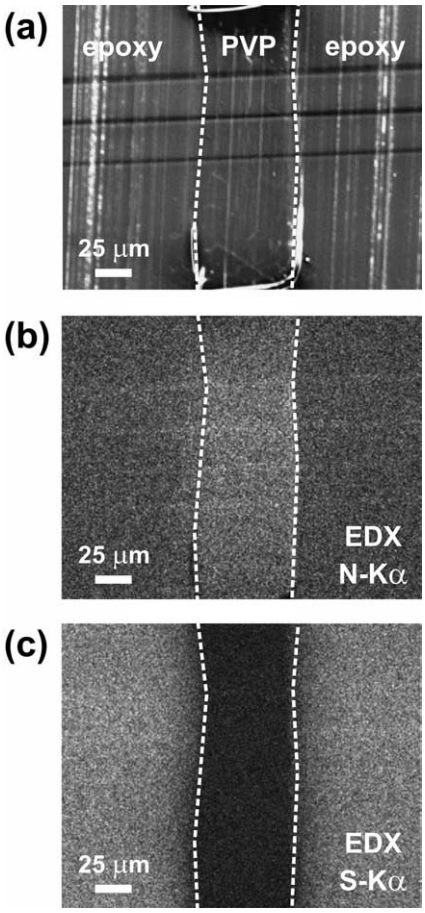

Fig. 2. (a) SEM micrograph showing the cross-section of an epoxy/PVP/epoxy sample. (b) Corresponding EDX map of the spatial variations of the N Kα peak. (c) EDX map of the spatial variations of the S Kα peak. Beam energy 11.0 keV. Maps: pixel resolution 256×200, dwell time per pixel 2 s.

interfacial borderlines from the more distant epoxy regions (in the following denoted as bulk epoxy), the decay of the S-signal intensity is more gradual rather than abrupt. The statement of an extended concentration decay can be made for the left-sided (epoxy/PVP) as well as for the right-sided (PVP/epoxy) region.

For purpose of determining the particular concentration profiles, the EDX measurements were also made in a line mode. The chosen lines were perpendicular to the interfacial borderlines. An example is shown in Fig. 3. In (Fig. 3(a)), the position of the line is marked with black arrows. By normalising the S- as well as the N-signal with the signal from the Ti Kα peak (Ti film thickness ~36 nm), distortions of the profiles by potential temporal variations of the electron beam current were avoided. Such variations cannot be fully ruled out due to the long signal accumulation times of several hours. The decay zones of the S/Ti-signal are clearly visible from (Fig. 3(c)) and are shadowed in a gray tone. For comparison, part of the map from (Fig. 2(c)) is given in (Fig. 3(d)). From the I_S/I_{Ti}-profile of (Fig. 3(c)),

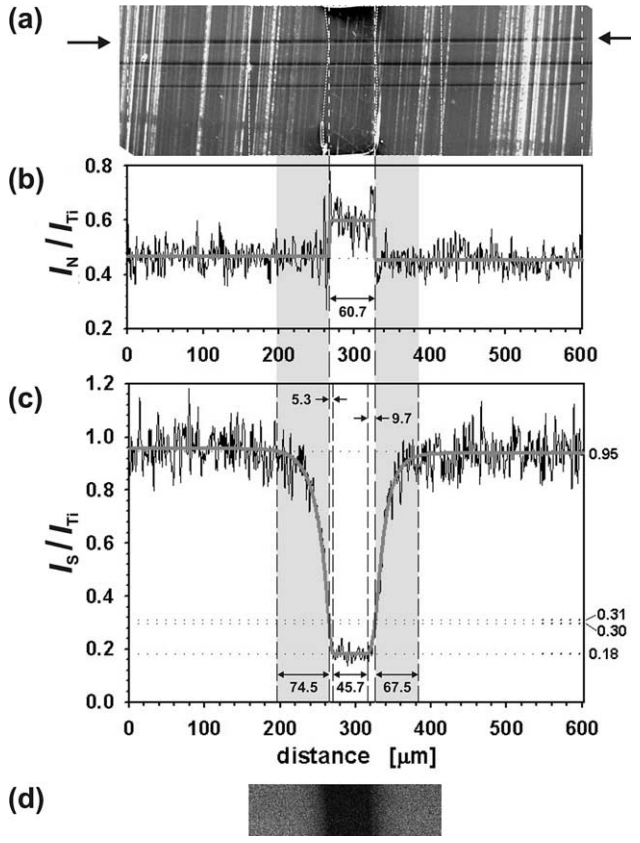

Fig. 3. Concentration profiles across the epoxy/PVP/epoxy interfaces, as measured by means of EDX. (a) SEM micrograph showing the position of the cross-sectional line (see arrows) for EDX analysis. The resulting profiles are given in (b) and (c), respectively. The total length of the profiles is 602 μm. The S- and the N-signals were divided by the signals from the Ti atoms in order to eliminate any variations in the electron beam intensity. From the I_N/I_{Ti}- profile steps are visible which were taken benefit of in order to deduce the edges of the PVP layer. However, the I_S/I_{Ti}- profile exhibits gradients extending over ~71 μm within the epoxy. Very clearly, within the PVP layer the S-concentration is non-zero. Profiles: 2048 data points, dwell time per data point 4 s. The data were slightly smoothed. The gray lines resulted from fit procedures. (d) For purpose of comparison, the upper part of the S-map displayed in Fig. 2(c). In (a), the location of the maps from Fig. 2 is indicated by the dashed white rectangle.

two major observations can be done: (i) In the vicinity of PVP (as identified by the high I_N/I_{Ti} signal), the concentration of DDS is significantly reduced (as compared to bulk epoxy) and the total width of the depletion zone is no less than 74.5 and 67.5 μm for the left- and the right-sided epoxy, respectively. (ii) Within PVP, the concentration of DDS is significantly larger than zero, thus indicating absorption of DDS molecules by the PVP layer.

In more detail, the concentration of DDS appears to be constant within the central part of the PVP film and shows some rise across the outer regions.

From Monte Carlo simulations for the given electron energy of 11.0 keV and the epoxy, it can be concluded that the lateral resolution of the EDX analysis is in the range of 2–3 μm, which corresponds to the lateral extent of the sub-surface electron scattering lobe. This resolution limit is much less than the detected widths of the DDS concentration decays within epoxy and even less than the comparatively narrow decays within the PVP regions.

In the following, the DDS concentration gradients within epoxy are referred to as 'chemical IPs'. This term serves as a differentiation from the modulus gradients (Section 5) which are referred to as 'mechanical IPs'. The corresponding IP widths are denoted as w_{DDS} and w_E, respectively. Even though the DDS concentration gradient may not be identical with gradients possibly deduced from other methods sensitive for the chemistry of the system (such as infrared spectroscopy), it reflects local deviations from the stoichiometric balance between amine and epoxy.

For translating the signal intensity profiles from EDX into the corresponding profiles of the amine–epoxy concentration ratio, a reference series of epoxy samples of well-defined r-values was analysed. In the case of these samples, the thickness of the Ti layer on top of the surfaces was ~34 nm. The EDX data are given in (Fig. 4(a)). However, the data did not cover the full range of signal intensity variations $0.3 \leq I_S/I_n \leq 1.0$ of the measured profile (Fig. 3(c)), and the linear extrapolation of the data delivered an unreasonable non-zero intensity for $r=0$ (dashed line in Fig. 4(a)). Thus a Monte Carlo simulation of the EDX experiment was performed in order to provide reference data over the full range of r-values.

As visible from (Fig. 4(a)), the simulation data fit to a large part of the measured data although some departure occurs at low r-values. The curve deduced from the simulation data exhibits a slight convex curvature and fulfils the condition of zero signal intensity for vanishing r. In a second step, the assumed thickness of the Ti cover layer was increased until the relative signal intensity for $r=1$ was equal to the measured one, namely $I_S/I_{Ti}=0.95$ (Fig. 3(c)). This condition was met for a Ti layer thickness of 37 nm which is in agreement with the microbalance reading of 36 nm. Then, respective simulations were performed for various r values and a characteristic curve determined. The final profile of the concentration ratio, as resulting from the application of this characteristic onto the signal intensity profile from (Fig. 3(c)) is shown in (Fig. 4(b)). Starting from the bulk epoxy value of $r \sim 1$, across the IP r decreases to ~0.27. Thus, a strong stoichiometric imbalance is generated within the epoxy IP through the absorption of DDS by the PVP film.

It should be noted, however, that the above approach of converting the DDS concentration into the amine–epoxy concentration ratio, r, is based on the assumption of negligible concentration variations of DGEBA. Although this approach may not be fully justified and some quantitative deviations from the true r-profile may exist, qualitatively the pronounced amine depletion can be expected to outweigh the epoxy concentration variations and to entail a drop of the concentration ratio r. Indeed, in their study involving brominated DGEBA, Oyama et al.

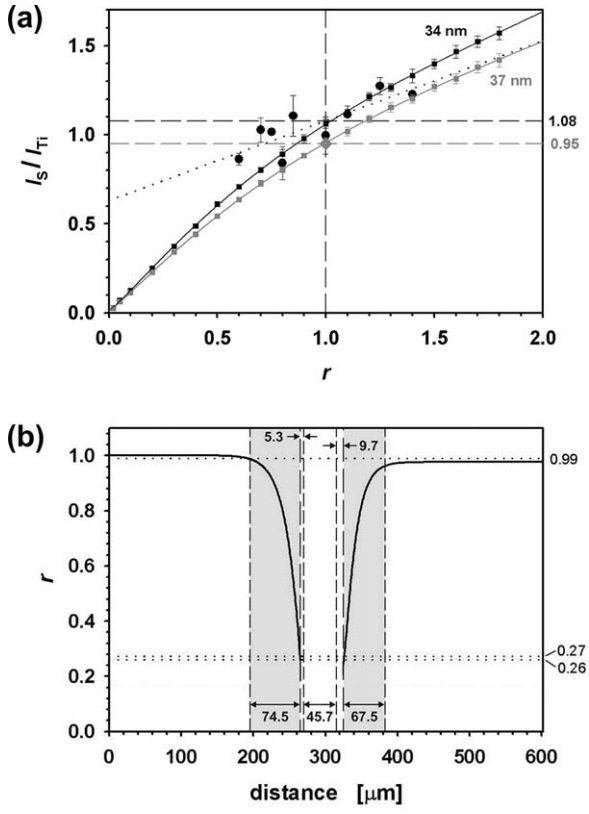

Fig. 4. (a) Relationship between the relative EDX signal intensity, I_S/I_{Ti}, and the molar concentration ratio, r. Measured data (circles) are compared with data resulting from Monte Carlo simulation (squares) employing the CASINO software [50–52]. The measured data resulted from a series of epoxy reference samples of well-defined r values; the scatter bars represent the standard deviation of the data. The simulation was done for two different values of the Ti film thickness: 34 and 37 nm, marked with black and gray squares, respectively. The corresponding solid lines are provided as a guide to the eye. The curve for the 34 nm case is a sufficient fit to the measured data from the concentration series. The curve for the 37 nm case, however, lies somewhat below the measurement values, but its value at $r=1$ is consistent with the bulk value of the profile given in Fig. 3(c). Whereas the linear extrapolation of the measured data (dotted line) gives a non-zero intensity at $r=0$, the simulated data show a non-linear characteristic which provides the required intensity decay down to zero. Obviously, in the case of the reference series the thickness of the Ti film was slightly lower. The value 37 nm for the Ti film thickness on the sandwich sample is in fair agreement with the value from the microbalance display, which was 36 nm. For converting the profile given in Fig. 3(c) into a corresponding concentration profile (see (b)), the curve for the 37 nm case was used.

[36] observed both a depletion of amine and of epoxy. For the system corresponding to the present case (initial curing for 2 h at 170 °C; PVP-K90), they found total transition widths of 24 and 72 μm, respectively. Thus, there exists a strong difference in the widths of the DDS concentration decays between the present study (on average, $w_{DDS}=71$ μm, see Fig. 3) and the study by Oyama et al. (24 μm). However, the smaller width observed in their study is consistent with the faster curing rate for their epoxy system containing a 1:1 mixture of standard and brominated DGEBA. According to the references [36,38], at a curing temperature of 175 °C the time required for 90% conversion is 57 min for an epoxy mixture with 40% of the brominated DGEBA and 226 min for the neat standard DGEBA. Thus, in the case of the latter system a much longer time is available for interdiffusion processes and wider IPs can be expected.

From the concentration profile a modulus profile can be calculated if the relationship $E(r)$ is known. Although this relationship is first of all required for the RT, temperature-dependent DMA was performed in order to allow a broader view and to develop a deeper understanding of the factors governing the viscoelastic properties of the epoxy.

4. Dynamic mechanical analysis (DMA) of an epoxy reference series

The viscoelastic properties of the epoxy are expected to change with the stoichiometric imbalance between epoxy resin and curing agent. In order to find out the details of the dependence, a concentration series of epoxy samples was investigated by means of DMA. Basically, this approach means approximating the amine concentration profile by a series of slabs of constant concentration ratios.

All the epoxy samples of the series were cured in the same manner (i.e. for 2 h at 170 °C), but differing in the amine–epoxy concentration ratio r. The r values of these samples ranged from 0.6 to 2.0. The respective DMA curves are given in Fig. 5. In each case the temperature was scanned from −180 °C to +270 °C (heating scan, see Fig. 5(a) and (b)) and back (cooling scan, Fig. 5(c) and (d)). The curves of the storage modulus, G', and of the loss modulus, G'', are displayed in Fig. 5(a)–(d), respectively. Three distinct features may be readily observed from (Fig. 5(a)): (i) A significant spread of the glass transition temperatures, T_α, ranging from ∼75 up to ∼200 °C; (ii) a pronounced variation of the storage modulus measured at RT, G'(20 °C) (as marked by a vertical dashed line at 20 °C); and (iii) a remarkable suppression of the β-transition (the centre of which is located between ∼−80 and ∼−60 °C). For each of the observations (i)–(iii), the variations are particularly pronounced for the samples with $r<1$. Within this regime, reduction of r results in a decrease of T_α, an increase of G' (20 °C), and a decrease of the relaxation strength of the β-transition. The latter finding is particularly obvious from the respective G'' curves (Fig. 5(b)), where the maximum value of the G''_β peak is notably reduced for $r<1$.

The changes of the glassy storage modulus G' with departure from the stoichiometric ratio $r=1$ are summarised in Fig. 6, where G' (20 °C) is plotted versus r. In the regime $r<1$ a pronounced increase of G' (20 °C) is observed with decreasing values of r. However, for the regime $r>1$ no significant changes of G' (20 °C) can be stated.

For purpose of comparison with the indentation experiments (Section 5), the shear modulus was converted into Young's modulus, E, assuming isotropic behaviour and a Poisson's ratio, ν, of 0.42 [53]. The Young's modulus is

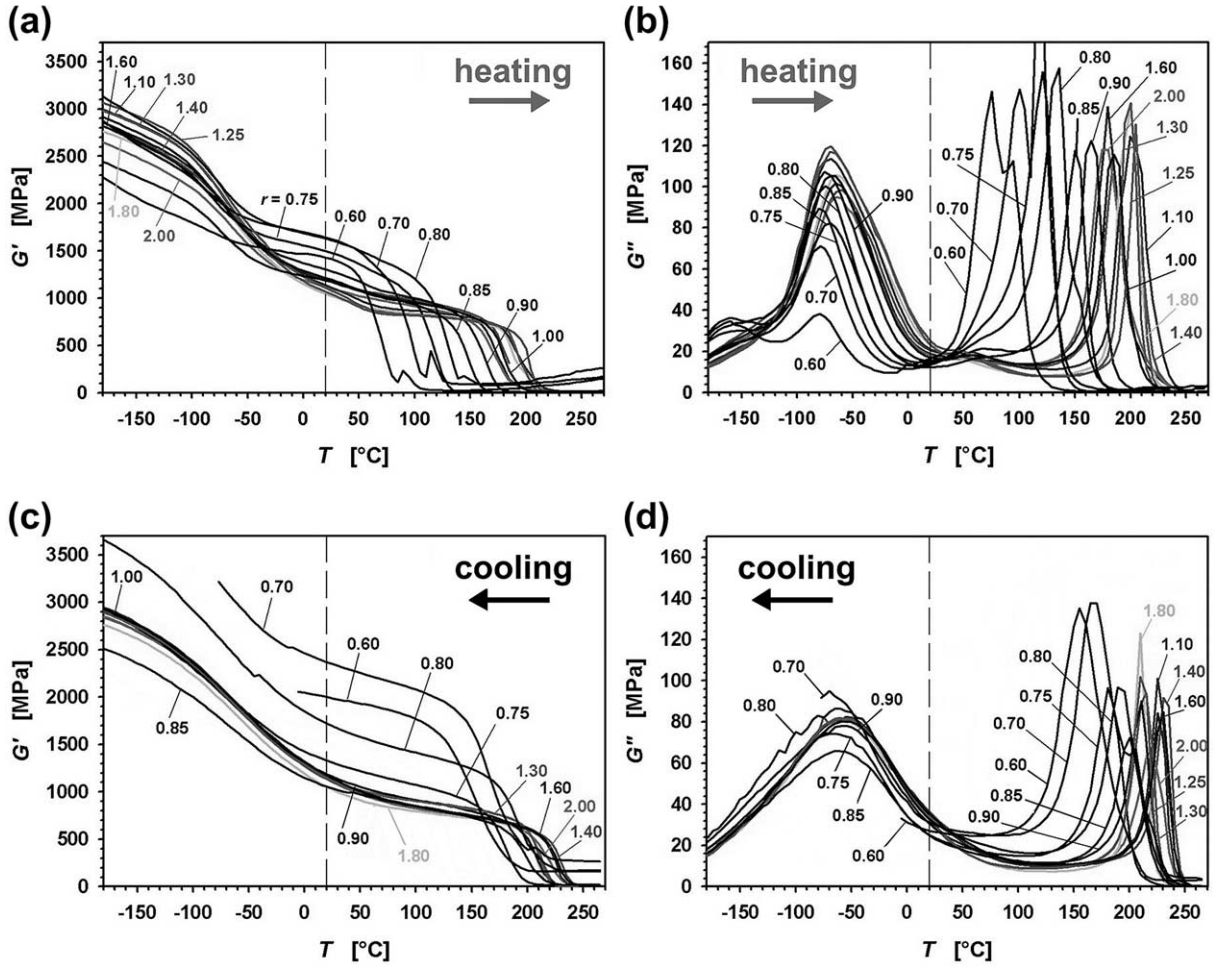

Fig. 5. Dynamic–mechanical analysis of the series of reference epoxy samples of different concentration ratios, r. The temperature range between −180 and +270 °C was scanned in both directions. The curves resulting from the heating and the cooling scans are shown in (a), (b) and (c), (d), respectively. (a) and (c) give the curves of the storage modulus, G', whereas (b) and (d) give the loss modulus, G''. Strong variations in the α-transitions (around 170 °C) can be observed between the samples of different r values. For the curves measured upon heating, pronounced variations of the β-transitions (around −70 °C) are also observed. As visible from (a), the storage modulus at RT (20 °C) is significantly increased for low values of r.

given by $E=2(1+\nu)G$ [54]. In terms of the Young's modulus, for the data from heating scans the total change between $r=1.0$ and $r=0.6$ is ∼1.0 GPa. Within the regime $r<1$, the relationship $E'(r)$ can be described by linear equations, both for the data from the heating and the cooling scans:

$$E'_{\text{heating}} = 6.0 - 2.6r \tag{2.1}$$

$$E'_{\text{cooling}} = 10.2 - 6.9r \tag{2.2}$$

In Section 5, Eq. (2.1) is used for converting the r-profile from (Fig. 4(b)) into a modulus profile (Fig. 10(b)).

The somewhat counter-intuitive result of increasing storage modulus with under-stoichiometric amount of amines cannot be exclusively explained in terms of the crosslink density, since the $T_\alpha(r)$-curve reflects a decrease of the crosslink density with increasing stoichiometric imbalance (see below). However, aside the crosslink density the elastic properties are also affected by the network topology and the corresponding packing density of elastically active bonds. In turn, the latter is expected to show a strong influence on molecular dynamics. The corresponding relaxation behaviour is reflected by the DMA measurements.

Similar observations were made by other authors studying off-stoichiometry effects in epoxies cured with aromatic amines. For the same system DER332/DDS, Meyer et al. [55] reported on a respective correlation, where the minimum modulus value occurred at $r=1$. In their case, the samples can be considered as fully cured since the curing schedule encompassed a post-curing step of 2 h at 220 °C. Skourlis and McCullough found a similar relationship for DGEBA cured with PACM 20, a cycloaliphatic diamine with a molecular weight of 340 [56]. It should be noted that also in these studies the increase on the excess-epoxy side is more pronounced than on the excess-amine side. In a similar manner, Drzal et al. observed a

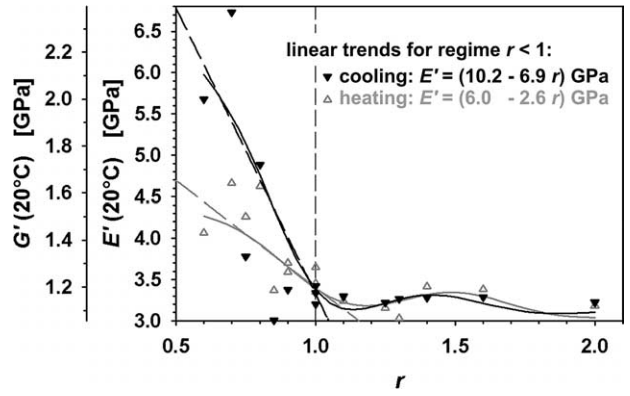

Fig. 6. Modulus–concentration relationship, as extracted from Fig. 5. The storage moduli, G' and E' are plotted as a function of r, both for the heating (gray) and the cooling (black) scans. The E' values were calculated from the G' values assuming isotropic behaviour. The solid lines are splines to the measured data. In the range $r<1$, the modulus values show a pronounced increase. The dashed lines represent linear approximations for the range $r<1$. The linear relationship deduced from the heating scan data is used for converting the concentration profiles from EDX (Fig. 4(b)) into modulus profiles (Fig. 10(b)). The minimum values occur slightly above the equimolar ratio, namely at $r\sim1.2$ (heating) and $r\sim1.1$ (cooling).

minimum epoxy stiffness around the stoichiometric ratio of a DGEBA-type epoxy resin cured with *meta*-phenylenediamine (*m*PDA) [4].

Concerning the glass transition temperature, T_α, and its changes with the concentration ratio r, a bell-shaped curve is found, with the maximum occurring around the concentration ratio $r\sim1.2$ (Fig. 7(b)). According to a widely accepted approach by Nielsen [23,56], T_α can be described in terms of the average molecular weight between crosslinks, M_c:

$$T_\alpha - T_{\alpha u} = \frac{C}{M_c} \tag{3}$$

where $T_{\alpha u}$ denotes the glass temperature of the uncured system and C a constant factor. Neglecting side reactions, a maximum crosslink density, $1/M_c$, is expected for fully cured stoichiometric systems, i.e. in the case, where all amine groups (primary as well as secondary ones) and epoxy groups are consumed by mutual reactions. However, in cases of a stoichiometric imbalance there remain either non-reacted epoxy groups (regime $r<1$) or non-reacted amine groups (regime $r>1$), thus resulting in a reduced average crosslink density. Due to their terminal position, non-reacted epoxy or primary amine groups represent dangling ends, each one of which comes along with an additional free volume. Hence, the total free volume is increased and results in a decrease of the glass transition temperature, T_α, with increasing deviation from the stoichiometric concentration ratio, $r=1$ [55–57]. These plasticisation effects are the stronger, the more reactive groups remain unconsumed.

In practice, the $T_\alpha(r)$ curve is frequently observed to be non-symmetric [57,58]. In the regime $r>1$, there remain

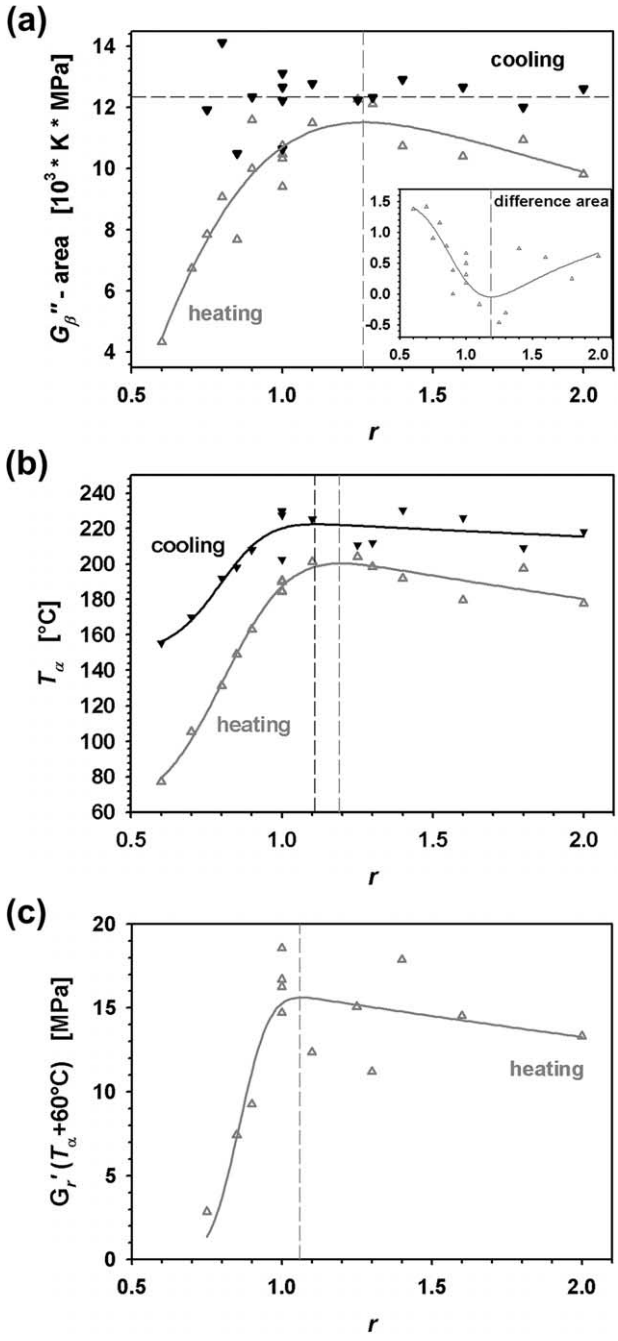

Fig. 7. Variation of three characteristic parameters with the concentration ratio, r: (a) The total area of the G''_β loss peak, (b) the glass transition temperature, T_α, and (c) the rubber modulus, $G'_r(T_\alpha+60\,°C)$. Each of these curves are bell-shaped with the maximum around $r\sim1.2$. The inset of (a) shows the difference between the total area of the G''_β loss peak and the area of the main G''_β loss peak (centred at $\sim-70\,°C$). The difference area is a measure of the strength of the $\tilde{\beta}$-transition, occurring at the low-temperature wing of the β-transition. Owing to its rise with increasing departure from the stoichiometric ratio, it can be attributed to dangling ends. In (b), the curve for the cooling scan is above the one for the heating scan, thus reflecting the increased crosslink density as a result of the post-curing taking place in the course of the measurement.

non-reacted primary or secondary amine groups. In general, primary amine groups exhibit a higher reaction rate than secondary amine groups [59]. If all the primary amine

groups react with epoxy groups, then there will remain no dangling ends of amine molecules, even without any reaction of the secondary amine groups [58]. In addition, considering their molecular structure non-reacted epoxy groups may provide a larger contribution to the increase of the free volume than incompletely reacted amine groups [57]. Thus, the case of excess amine is expected to show less strong an effect on the resulting network structure than the case of excess epoxy.

Beyond these free volume effects, in principle another contribution may originate from the dependence of the curing kinetics on the amine concentration ratio [60]. Thus, the degree of cure reached after 2 h at 170 °C can depend on the value of r. In addition to the variations in the total amount of liberated exothermic heat, Finzel et al. [60] reported for the system DGEBA/DDS a side reaction, occurring under the conditions of excess epoxide and low temperature. The side reaction did not show a significant exothermic heat. It was attributed to the formation of a quaternary ammonium–alkoxide ion pair, resulting from the reaction between DGEBA and tertiary amine. However, the ion pair did not affect the T_α value, thus indicating that it is not a true crosslink but an equilibrium-limited species.

In a similar manner to T_α, the variation of the crosslink density can also be observed from the rubber modulus [23]. Indeed, a plot of the rubber storage modulus as measured at $T_\alpha + 60$ °C (Fig. 7(c)) delivered a similar curve to that of $T_\alpha(r)$ displayed in (Fig. 7(b)).

Another indication of dangling epoxy groups appears to be the emergence of a second loss peak (centred at ~ -160 °C) in the region of the β-transition. In particular, this observation is made for samples with $r<0.8$ (Fig. 5). Taking into account its almost separated appearance, in the following we refer to this peak as $\tilde{\beta}$-transition.

Indeed, the DMA curves (Fig. 5) exhibit significant differences in the strength of the β-relaxation. Owing to the partial suppression of the β-transition for the samples with $r<1$, the RT modulus of these samples is higher than that of the samples exhibiting a strong β-transition. Even though the storage modulus as measured below the β-transition is the lowest for the samples with $r<1$, their respective RT modulus is the highest. This effect is reflected by the crossing of the $G'(T)$-curves in the high-temperature region of the β-transition.

Considering the importance of the β-transition, it deserves a more detailed analysis. The changes of the centre temperature, T_β, as well as the full width at half magnitude (FWHM), ΔT_β, of the β-transition are given in Fig. 8. With decreasing values of r (regime $r<1$), the β-transition shifts to lower temperatures and its total width decreases. The DMA curves (Fig. 5) reveal that it is mainly the high-temperature part of the β-transition which is suppressed. This effect can also be readily observed from a plot of the area of the G''_β peak, as given in (Fig. 7(a)). For the data measured upon heating, the curve is bell-shaped with the maximum located at $r\sim 1.3$. Thus, it is similar to the corresponding curves of T_α and $G'_r(T_\alpha + 60\ °C)$, given in Fig. 7(b) and (c), respectively. Also from this similarity, a relationship to the crosslink density can be inferred.

As visible from the inset in (Fig. 7(a)), the difference between the total area of the G''_β peak and the fit curves (not shown) to the main G''_β peak (which is centred at ~ -70 °C) increases with the departure from the concentration ratio $r\sim 1.2$. This result reflects the existence of dangling ends and their particular dynamics, which becomes the more relevant the larger the degree of off-stoichiometry. Notably, a significant contribution from dangling end motions occurs for the excess-epoxy regime as well as for the excess-amine regime, although in the latter regime the effect is less pronounced. Taken this together with the asymmetry of the $T_\alpha(r)$-curve (Fig. 7(b)), this may indicate that non-reacted ends of the DGEBA molecules show a much stronger effect on the elastic network properties than non-reacted or only partially reacted ends of the DDS molecules.

The molecular dynamics of dangling epoxy groups can be expected to be rather local and easier to be activated than segmental motions severely restricted by the network of crosslinks. Indeed, the β-transition is frequently assigned to motions of the hydroxypropylether sequence (–CH_2–CHOH–CH_2–O–), see [61] and references therein. These sequences result from the addition reaction of epoxy groups with amines, and their dynamics should be more restricted than that of dangling epoxy groups.

As discussed by Halary et al. [62], the high-temperature part of the β-transition is related to a sort of local-scale cooperative motions. Consequently, the proportion of such cooperative motions is expected to decrease if the connectivity of the network is reduced, i.e. if the constraints imposed by the network structure are partially released. The connectivity in turn is given by the crosslink density. In that sense, the observed suppression of the high-temperature part of the β-transition can be considered as a result of the reduced crosslink density. Consistently with the above reasoning, Calventus et al. [57] deduced from their calorimetric study of the α-transition that the lower limit for the size of the cooperatively rearranging regions is greater for the stoichiometric system. In other words, off-stoichiometry implies that a smaller number of chain segments is involved in the relaxation process.

For the DMA curves measured upon cooling, to some degree the situation is different. As visible from Fig. 5(c) and (d) as well as from (Fig. 7(b)), the variations of T_α with r are not as strong as for the case of the heating scans. In the course of the measurement, T_α is exceeded and post-curing takes place as long as the curing reaction is no more diffusion-controlled. As a result, the average crosslink density increases and the number of dangling ends is reduced. Consistently, in the cooling scan the glass transition occurs at higher temperatures (Fig. 7(b)). Furthermore, the variations of T_α with r are less pronounced and the maximum of the curve is slightly shifted to lower r values (from $r\sim 1.2$ to 1.1). Concerning the β-transition, its

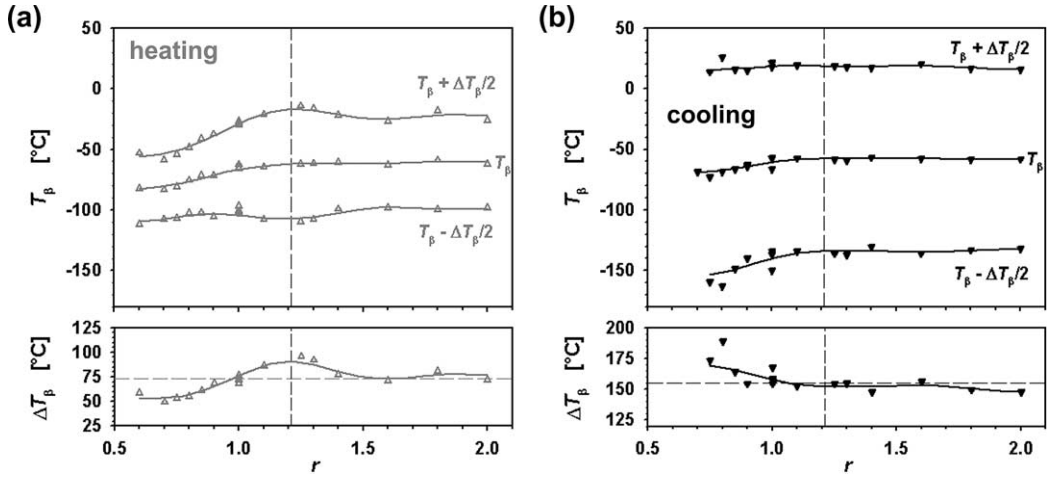

Fig. 8. Variation of the β-transition with the concentration ratio, r. In the upper graphs, the characteristic temperatures $T_\beta - \Delta T_\beta/2$, T_β, and $T_\beta - \Delta T_\beta/2$ are shown. In the lower graphs, the respective FWHM values, ΔT_β, are displayed. The changes are given for both the heating (a) and the cooling (b) scans, respectively. For the heating scan, the largest FWHM is observed for $r \sim 1.2$. For $r < 1$, T_β as well as ΔT_β decrease with increasing offset from the stoichiometric ratio $r = 1$, i.e. a suppression of the β-transition is observed.

width is much larger and it exhibits only little changes (Fig. 8(b)). This is also obvious from the corresponding curve of the total area of the G''_β peak (Fig. 7(a)). Although the cooling scans could not be finished for the samples with $r = 0.6$ and $r = 0.7$ due to technical reasons, from the available scans there are no indications of $\tilde{\beta}$-transitions (Fig. 5(d)). Considering the moderate changes of the β-transition with the concentration ratio r, within the regime $r < 1$ the variations of the storage modulus at RT, G' (20 °C), are astonishingly strong (Fig. 6, data from cooling scans). In the regime $r > 1.0$, however, no significant differences to the values from the heating scans can be stated. Notwithstanding the large strength of the β-transition, within the regime $r < 1.0$ the $G'(20\,°C)$ values measured upon cooling are higher than those measured upon heating. Thus, there must be reasons other than an antiplasticisation effect for the strong increase of $G'(20\,°C)$ with decreasing values of r (regime $r < 1$). One reason may be a different network topology, which provides a large density of elastically loadable bonds. Beyond the chemical crosslinks, also entanglements trapped by a high degree of topological constraints may be present which can give an additional contribution to the elastic modulus [63]. Another reason may be side-reactions, which provide additional crosslinks. As mentioned above, for excess-epoxy formulations of the system DGEBA-DDS cured at temperatures lower than $T_{\alpha\infty}$ (such as 160 °C), Finzel et al. reported on the formation of a quaternary ammonium–alkoxide ion pair by the reaction of epoxy groups with tertiary amines [60].

Although these findings deduced from the cooling scans may be of their own interest, in the present study the results from the heating scans are of major concern, since the curing of the epoxy/PVP/epoxy sandwich samples was done solely at 170 °C.

5. Modulus mapping across the epoxy interphase

The concentration gradient of the amine curing agent is expected to result in a corresponding gradient of the epoxy Young's modulus. For purpose of mapping local variations in mechanical properties, micro-scale indentation experiments were performed. The indents were arranged in lines with orientation perpendicular to the interfacial borderline between epoxy and the PVP layer. Within the indentation lines, the average and the lowest distance between neighboured indents were 15.0 and 8.9 μm, respectively. The total extent of the field of indentations was $\sim 810 \times 170\ \mu m^2$. At each indentation point a force-penetration curve, $P(h)$, was recorded and evaluated. According to the procedure developed by Oliver and Pharr [47], the upper portion of the unloading curve was described using the relationship

$$P = A(h - h_f)^m \tag{4}$$

where the constants A, m, and h_f were determined by a least squares fitting procedure. h_f denotes the depth of the remaining surface deformation. A review of the basics of the Oliver and Pharr theory was given by Fischer-Cripps [48]. The initial unloading slope is then found by evaluating the derivative of Eq. (4) at the peak load and displacement. This procedure delivers the reduced Young's modulus E_r of the tip-sample contact. From E_r, the sample modulus, E_s, was calculated using the values $E_t = 1140$ GPa and $\nu_t = 0.069$ for the diamond Young's modulus and Poisson's ratio, respectively, and $\nu_s = 0.42$ for the epoxy Poisson's ratio [53]. The relationship between E_r, E_s, and E_t is given by Ref. [47]:

$$\frac{1}{E_r} = \frac{1 - \nu_s^2}{E_s} + \frac{1 - \nu_t^2}{E_t} \tag{5}$$

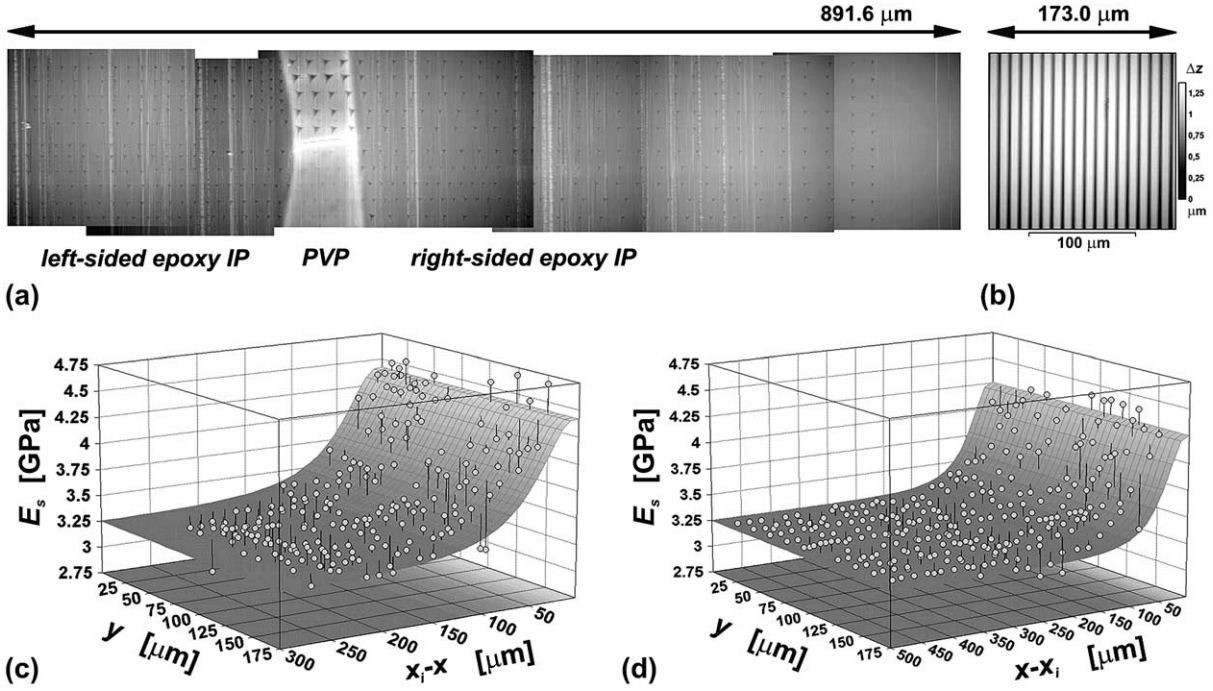

Fig. 9. (a) Topography image of the field of indentations, recorded after the indentation experiments were finished. For covering the large field of indentations, several topography images taken at different positions were stitched together. The PVP surface appears bright, because its altitude is higher than that of the epoxy surface. (b) For purpose of reference, a topography image measured on a Si calibration grating (pitch size 10 μm) is shown. (c) Pseudo-3D-plot of the spatial distribution of the sample Young's modulus values, E_s, measured on the left-sided epoxy IP. The distance from the epoxy–PVP borderline is denoted as $x_i - x$. (d) Like (c), but for the right-sided epoxy IP. $x - x_i$ denotes the distance from the borderline between PVP and epoxy.

After a series of indentation experiments at pre-defined positions was completed, the resulting field of indentation marks was imaged in a scanning mode. Since the total extent of the indentation field is larger than the maximum scan range of ~173 μm, the scan field was successively translated and the resulting topography images were stitched together (Fig. 9(a)). For each line of indents, the cross-section with the interfacial borderline was determined. For each indentation mark of a given line, the distance $|x_i - x|$ from the point of cross-section, x_i, was calculated.

From the stitched topography image (Fig. 9(a)), the PVP layer may be readily observed owing to the fact that its surface is at a higher altitude than that of the epoxy. This finding can be attributed to some swelling of the PVP due to uptake of water from the air. PVP is a hygroscopic substance, exhibiting an absorption behaviour largely independent of the molecular weight [39]. On the contrary, the topography of the cross-sectioned surface, as measured soon after microtoming was finished, did not exhibit a discernible height step between epoxy and PVP. Indeed, in the course of the first indentation experiments the identification of the PVP layer was achieved through the much larger plastic deformation of PVP rather than through topographic features.

An eye-catching feature of (Fig. 9(a)) is the strong difference in the size of the indentation marks on PVP, since the marks in the upper five lines are much more pronounced than the ones in the lower five lines. This is due to the fact that these measurements were performed four weeks later than the first series of indentation lines. As indicated by the different plastic deformation behaviour, in the meanwhile the hygroscopic PVP layer had absorbed some water from the air, although the sample was stored in an exsiccator providing a reduced humidity. As a result of the water uptake, the PVP hardness was decreased. On epoxy, however, the indentation experiments of the upper five rows did not show differences to the experiments of the lower five rows.

The plots of the epoxy Young's modulus values, E_s, versus the lateral position of the indentation are given in Fig. 9(c) and (d). With decreasing distance $|x_i - x|$ from the interface, there occurs a significant increase of E_s. The epoxy bulk modulus value, i.e. the epoxy modulus at a distance far away from the IP is (3.25 ± 0.07) GPa. The total modulus change from the region more than 300 μm away from the interface to the position at $x = x_i$, is ~1.1 GPa.

It should be noted that interface-related artefacts of the indentation experiments can be widely ruled out, owing to the vast extent of the modulus decay. From the principal point of view, indentations in the close vicinity of a neighboured phase can be affected by its mechanical properties. This is a consequence of the lateral extent of the sub-surface stress distribution. For instance, a corresponding analysis at an interface between poly(carbonate) (PC) and steel has shown that the apparent modulus measured on PC is increased at distances, d, lower than

the diameter of the final indentation mark [46]. Hereby, d denotes the distance between the centre axis of the indenter and the interfacial borderline. This condition is met across all the indentation field on the epoxy/PVP/epoxy cross-section. Furthermore, the Young's modulus value measured on PVP is $E_s \sim 3.9$ GPa (as calculated for a PVP Poisson's ratio of $\nu_s \sim 0.35$) which is even lower than the epoxy modulus value measured in the close vicinity of the interfacial borderlines. That is, if there existed a measurement artefact at all, it should result in too low a measured epoxy modulus value rather than a too large one. However, E_s was observed to increase in a monotonic manner with decreasing distance $|x_i - x|$. In (Fig. 10(a)) average modulus profiles are given which resulted after all the $E_s(x, y)$ data were projected onto the E_s versus $|x_i - x|$-plane and a smoothing procedure was applied. The corresponding profiles for the left-sided and the right-sided epoxy IP are very similar to each other, although the E_s values on the right IP are slightly larger. The average profile is extended over 175.1 μm. It should be noted that the position of the demarcation line between IP and bulk epoxy was defined by a deviation of 1% from the bulk value of E_s. The limiting value was not set more strictly, in order to make the determination of the IP width less dependent on the asymptotic behaviour.

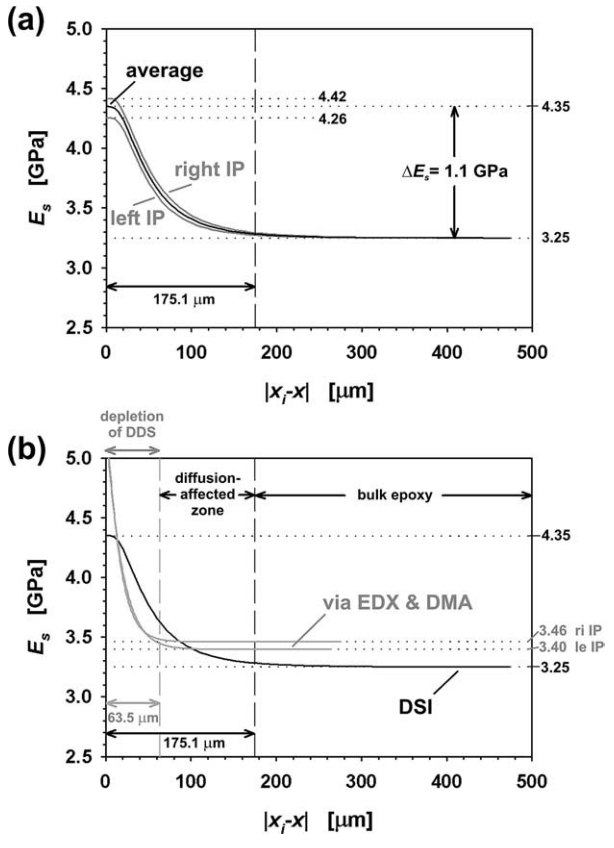

Fig. 10. (a) Smoothed data from Fig. 9(c) and (d), after projection onto the distance axis $|x_i - x|$. The profiles of the left and the right IPs are very similar to each other. The black line represents the average of both decays. The total width of the average decay is $w_E \sim 175.1$ μm. (b) The average modulus profile (approach B) is compared to the modulus profiles deduced from the EDX and the DMA data (approach A). Both approaches show a modulus increase with decreasing distance, $|x_i - x|$, from the interface. However, the measured modulus decay (i.e. via DSI) is ~2.8 times wider than the decay resulting from the concentration gradient (width 63.5 μm).

The average profile of E_s derived from the indentation experiments (approach B) can be compared to the modulus profiles deduced from the combined EDX and DMA analysis (approach A), see (Fig. 10(b)). Both results are in qualitative agreement since they both exhibit an increase of E_s with decreasing distance $|x_i - x|$ from the interfacial borderline. The major differences are given by the final modulus values and the total width of the modulus decay. Concerning approach A, it should be noted that the modulus values at distances $|x_i - x| < 20$ μm resulted from an extrapolation of the linear trend valid within the range $0.6 < r < 1$ to the range $r < 0.6$ (Fig. 6). Thus, the calculated modulus increase may be different from the real one. The scatter of the data implies a non-negligible error in the E_s data from approach A. The value of the Poisson's ratio, ν_s, used for converting from shear to Young's modulus can give an additional contribution to the total error. The used value of $\nu_s = 0.42$ was taken from literature [53].

The width of the decay, however, is affected solely by the respective precision of the EDX profiles, which is ~1 μm. Hence, the stunning difference in the mechanical IP widths of 63.5 (approach A) and 175.1 μm (approach B) cannot be attributed to measurement errors. Instead, rather than being a mere reflection of the amine concentration decay, it can be inferred that the mechanical IP must be influenced by additional effects. Moreover, the fact that the measured modulus decay is ~2.8 times wider than the one deduced from the DDS concentration decay indicates that these additional effects are of a more long-range nature.

6. Discussion

As mentioned in Section 3, for their system corresponding to the one of the present study (initial curing for 2 h at 170 °C; PVP-K90), Oyama et al. [36] reported on total widths of 24 and 72 μm for the DDS and the brominated DGEBA concentration decays, respectively. Although both the curing rate is higher for epoxy systems including brominated DGEBA and the DDS concentration decay is much wider in the present case (on average $w_{DDS} \sim 71$ μm, Fig. 3), the ratio of $w_E/w_{DDS} \sim 2.5$ (between the decay widths of the epoxy modulus and the DDS concentration) is similar to the ratio of ~3.0 between the decay widths of the brominated DGEBA and the DDS concentration given in Ref. [36]. Thus, there exists some indication that the wide mechanical IP may be attributed to a possibly existing concentration decay of the epoxy resin. Moreover, a moderate depletion of DGEBA superimposed to the strong depletion of DDS would still result in a local increase of the concentration ratio, r, but a less pronounced one than that

calculated solely from the DDS concentration profiles (Fig. 4(b)). As a consequence, the corresponding rise in epoxy modulus should be more gradual, in agreement with the measured modulus profiles (Fig. 10(b)). Within the diffusion-affected zone, a slight depletion of DGEBA combined with a bulk-like concentration of DDS would result in values of $r>1$, i.e. with amine in excess. However, as visible from Fig. 6, for the given system the minimum of the $E(r)$-relationship occurs for $r\sim1.2$. This means that as compared to $r=1$, within the range $1.0<r<1.2$ the modulus is expected to decrease before it increases again slightly for values of $r>1.2$. Thus, given the $E(r)$ relationship displayed in Fig. 6, the assumption of epoxy depletion results in a non-monotonic modulus profile, a consequence which is inconsistent with the observed modulus profiles. Considering the limited number of data in Fig. 6, however, the relationship $E(r)$ should not be over-stressed, in particular in the range around the minimum. Nevertheless, there may exist other reasons for the extended mechanical IP.

Essentially, the locally increased epoxy stiffness reflects a higher local crosslink density or a higher packing density of elastically loadable bonds. Both may result from the diffusional currents induced by the interdiffusion taking place during the curing procedure: Driven by the absorption of amine molecules by the PVP layer, within the adjacent epoxy layer a depletion of amine molecules occurs. The corresponding concentration gradient leads to net diffusional currents of amine molecules from the bulk epoxy formulation toward the interface. Thus the diffusional motion of the amine molecules is enhanced over that of the isotropic Brownian motion, which increases the collision rate with potential reaction partners. Given a certain reaction probability upon collision between amine and epoxy groups, the local crosslink density is expected to be higher than that of the epoxy, where the curing was not affected by any interface-induced diffusion processes.

Furthermore, the final network topology can also be affected. Already existing topologic constraints on the molecular mobility may be mitigated by the interdiffusion processes. The adverse effect of a high crosslink density on the packing efficiency is known from various experiments, see Ref. [64] and the references therein. Thus, in many cases it seems that the units, which form the network inhibit close packing because of steric restrictions. In other words, a high crosslink density can imply a large free volume of the final network. For instance, cage-like effects are related to a lower overall packing density, since the dense network surrounding a comparatively unoccupied volume (the cage) provides too large a barrier for further amine molecules to enter and add further crosslinks inside. However, by the action of a driving force toward the region of reduced amine concentration, some diffusion barriers become more likely to be surpassed and the probability for accessing the respective free volumes is increased.

Via such effects related to anisotropic diffusion, much wider an epoxy volume can be affected than the IP volume exhibiting amine depletion. Also in this sense, the mechanical IP can be sub-divided into a DDS depletion zone ($r<1$) and a solely diffusion-affected zone ($r=1$), see (Fig. 10(b)).

In the case that the effect on crosslink density outweighs the effect on packing density, a profile of the local glass transition temperature, T_α, should show a maximum in the intermediate region, where $r\sim1$ (such as in bulk epoxy) is combined with the occurrence of an increased crosslink density. It is interesting to note, that if the sample was post-cured and the value $T_{g\infty}$ was reached, such local variations of T_α within stoichiometric epoxy should be eliminated.

Moreover, within the diffusion zone the curing kinetics should also be affected, since completely non-reacted amine molecules are the smallest entities and are expected to exhibit the highest mobility. These non-reacted amine molecules, however, carry two primary amine groups which in turn are known to show the highest reaction rate with the epoxy groups [59].

7. Conclusions

A study of the interphase between the thermoplastic poly(vinylpyrrolidone) (PVP) and an amine-cured epoxy was performed. A stoichiometric amine–epoxy formulation was cured in the presence of a PVP film. The curing was done for 2 h at a temperature of 170 °C which is close to the glass transition temperature, T_α, of the PVP. Sandwich-like samples of the sequence epoxy/PVP/epoxy were prepared.

Employing energy-dispersive analysis of X-rays (EDX) and depth-sensing indentation (DSI), cross-sections of such samples were investigated for providing maps of the local amine concentration and the local Young's modulus, respectively. The S atom of 4,4′-diaminodiphenylsulfone (DDS) was used for tracking local concentration variations of the curing agent. Within PVP, a non-zero concentration of DDS was found as well as an adjacent zone of amine depletion within epoxy. The width of this zone was $w_{DDS}\sim71$ μm. This shows that a significant amount of amine was absorbed by the central PVP layer, resulting in stoichiometric imbalances in the epoxy adjacent to the PVP film surface. Such interdiffusion processes are most likely in the early phase of the curing reaction when the viscosity of the liquid formulation is still low.

On the other hand, quite a number of indentation experiments on a field of 892×110 μm^2 have shown a strong increase of the epoxy modulus when approaching the interface from the bulk. Across this mechanical interphase, the total change of the Young's modulus, E_s, is ~1.1 GPa, and the total width is $w_E\sim175$ μm. Thus, the local amine depletion detected via EDX corresponds to increased modulus values. The total width of the chemical interphase,

however, is ~2.5 times lower than that of the mechanical interphase.

For purpose of working out the correlation between amine concentration and epoxy stiffness, a series of epoxy samples of different amine–epoxy concentration ratios, r, was investigated by means of temperature-dependent dynamic mechanical analysis (DMA). In consistency with the mapping results, for the regime with epoxy in excess ($r<1$) the room temperature modulus was observed to rise with increasing deviation from the stoichiometric ratio ($r=1$). This somewhat counter-intuitive observation can be attributed to a suppression of the β-transition around −70 °C. The so-called antiplasticisation effect is well-known from literature and was ascribed to the attenuation of local-scale cooperative motions with decreasing crosslink density.

The large width of the mechanical interphase indicates that the modulus variations are not solely caused by the local concentration variations of the amine curing agent. One reason can be that also spatial variations of the epoxy concentration exist, extending over a range wider than the amine depletion zone and inducing corresponding variations of r. Indeed, Oyama et al. [36] observed some depletion of their brominated DGEBA over distances ~3 times wider than the amine depletion zone. Another likely reason for the vast extent of the modulus gradient may be that the curing reaction was affected by the diffusion of amine molecules from the bulk to the region of amine depletion. These long-range diffusion currents can interfere with the curing, e.g. by enhancing the likelihood of an amine group to encounter an epoxy group and to react with each other. Thus, between the zone of amine depletion and the bulk epoxy, a zone of diffusion-affected epoxy can be expected, characterised by an increased crosslink density.

After all, it was shown that pronounced interphases may occur between thermoplastic components and amine-cured epoxy. The observations provide evidence for the inter-diffusion concept. Beyond the furthering of the fundamental understanding of interphasial phenomena, in engineering applications the calculation of interfacial stress distributions within composites may benefit from the detailed knowledge of modulus gradients.

Acknowledgement

Some of the EDX data were collected by G. Eltanany in the frame of her PhD studies, which she did not continue, however. We gratefully acknowledge her contribution. Furthermore, we express our gratitude to P. Fengler (BAM VI.1) for careful performance of the DMA measurements and to D. Neubert (BAM, VI.11) for running the DSC as well as the TGA experiments. M.M. was involved into a project related to exchange of researchers (PPP) with Spain, funded by the German Academic Exchange Service (DAAD). He would like to express his gratitude to Prof I. Mondragon and his working group (Department of Chemical Engineering, University of the Basque Country, San Sebastian, Spain) for valuable discussions on epoxy characterisation. A sample of the epoxy resin DER332 was kindly provided by Nordmann-Rassmann GmbH.

References

[1] Stamm M, Schubert DW. Annu Rev Mater Sci 1995;25:325–56.
[2] Varga J, Karger-Kocsis J. Compos Sci Technol 1993;48:191–8.
[3] Lustiger A, Marzinsky CN, Mueller RR, Wagner HD. J Adhes 1995; 53:1–14.
[4] Drzal LT, Rich MJ, Koenig MF, Lloyd PF. J Adhes 1983;16:133–52.
[5] Williams JG, James MR, Morris WL. Composites 1994;25:757–62.
[6] Wagner HD, Lustiger A. Composites 1994;25:613–6.
[7] Nath RB, Fenner DN, Galiotis C. J Mater Sci 1996;31:2879–83.
[8] Adams RD, Singh MM. Compos Sci Technol 1996;56:977–97.
[9] Hodzic A, Stachurski ZH, Kim JK. Polymer 2000;41:6895–905.
[10] Papanicolaou GC, Theocaris PS. Colloid Polym Sci 1979;257: 239–46.
[11] Theocaris PS, Spathis GD. J Appl Polym Sci 1982;27:3019–25.
[12] Mamunya YP, Davydenko VV, Pissis P, Lebedev EV. Eur Polym J 2002;38:1887–97.
[13] Kawaguchi T, Pearson RA. Polymer 2003;44:4239–47.
[14] Lee A, Lichtenhan JD. Macromolecules 1998;31:4970–4.
[15] Choi J, Harcup J, Yee AF, Zhu Q, Laine RM. J Am Chem Soc 2001; 123:11420–30.
[16] Zhang MQ, Rong MZ, Yu SL, Wetzel B, Friedrich K. Wear 2002;253: 1086–93.
[17] Nelson JK, Fothergill JC. Nanotechnology 2004;15:586–95.
[18] Broyles NS, Chen R, Davis RM, Lesko JJ, Riffle JS. Polymer 1998;39: 2607–13.
[19] Oyama HT, Wightman JP. Surf Interface Anal 1998;26:39–55.
[20] Gilbert AH, Bucknall CB. Macromol Symp 1991;45:289–98.
[21] Crank J. The mathematics of diffusion. 2nd ed. Oxford: Clarendon Press; 1975 [chapter 10].
[22] Rajagopalan G, Narayanan C, Gillespie Jr JW, McKnight SH. Polymer 2000;41:8543–56.
[23] Nielsen LE. J Macromol Sci-Rev Macromol Chem C 1969;3:69–103.
[24] Anifantis NK. Compos Sci Technol 2000;60:1241–8.
[25] Suresh S, Mortensen A. Int Mater Rev 1997;42:85–116.
[26] Lambros J, Santare MH, Li H, Sapna III GH. Exp Mech 1999;39: 184–90.
[27] Rajagopalan G, Immordino KM, Gillespie Jr JW, McKnight SH. Polymer 2000;41:2591–602.
[28] Lestriez B, Chapel J-P, Gérard J-F. Macromolecules 2001;34: 1204–13.
[29] Yun NG, Won YG, Kim SC. Polymer 2004;45:6953–8.
[30] Kinloch AJ, Little MSG, Watts JF. Acta Mater 2000;48:4543–53.
[31] Lesko JJ, Jayaraman K, Reifsnider KL. Key Eng Mater 1996;116/117: 61–86.
[32] VanLandingham MR, McKnight SH, Palmese GR, Bogetti TA, Eduljee RF, Gillespie Jr JW. Mater Res Soc Symp Proc 1997;458: 313–8.
[33] Munz M, Sturm H, Schulz E, Hinrichsen G. Compos A 1998;29: 1251–9.
[34] Gao S-L, Mäder E. Compos A 2002;33:559–76.
[35] Munz M, Cappella B, Sturm H, Geuss M, Schulz E. Adv Polym Sci 2003;164:87–210.
[36] Oyama HT, Lesko JJ, Wightman JP. J Polym Sci B 1997;35:331–46.
[37] Oyama HT, Solberg TN, Wightman JP. Polymer 1999;40:3001–11.
[38] Naé HN. J Appl Polym Sci 1987;33:1173–85.

[39] Bühler V. Kollidon-polyvinylpyrrolidone for the pharmaceutical industry. 6th ed. Ludwigshafen: BASF-Pharma Ingredients; 2001 [chapter 2].
[40] Product manual: DOW liquid epoxy resins. Midland: DOW Plastics; 1999.
[41] White SR, Mather PT, Smith MJ. Polym Eng Sci 2002;42:51–67.
[42] Mathieu C, Boiteux G, Seytre G, Villain R, Dublineau P. J Non-Cryst Solids 1994;172–174:1012–6.
[43] Scheirs J, Bigger SW, Then ETH, Billingham NC. J Polym Sci B 1993;31:287–97.
[44] Remiro PM, Cortazar MM, Calahorra ME. J Mater Sci 1999;34: 2627–33.
[45] Tan YY, Challa G. Polymer 1976;17:739–40.
[46] Munz M, Chung J, Kalinka G. Mapping epoxy interphases. In: Possart W, editor. Adhesion—current research and applications. Weinheim: Wiley; in press [chapter 8].
[47] Oliver WC, Pharr GM. J Mater Res 1992;7:1564–83.
[48] Fischer-Cripps AC. Vacuum 2000;58:569–85.
[49] Briscoe BJ, Fiori L, Pelillo E. J Phys D 1998;31:2395–405.
[50] Hovington P, Drouin D, Gauvin R. Scanning 1997;19:1–14.
[51] Drouin D, Hovington P, Gauvin R. Scanning 1997;19:20–8.
[52] Hovington P, Drouin D, Gauvin R, Joy DC, Evans N. Scanning 1997; 19:29–35.
[53] Verdu J, Tcharkhtchi A. Angew Makromol Chem 1996;240:31–8.
[54] Kuchling H. Taschenbuch der Physik. 5–7th ed. Thun: Verlag Harri Deutsch; 1985 [chapter 12].
[55] Meyer F, Sanz G, Eceiza A, Mondragon I, Mijovic J. Polymer 1995; 36:1407–14.
[56] Skourlis TP, McCullough RL. J Appl Polym Sci 1996;62:481–90.
[57] Calventus Y, Montserrat S, Hutchinson JM. Polymer 2001;42: 7081–93.
[58] Yim H, Kent M, McNamara WF, Ivkov R, Satija S, Majewski J. Macromolecules 1999;32:7932–8.
[59] Lee H, Neville K. Handbook of epoxy resins. New York: McGraw-Hill; 1967 [chapter 8].
[60] Finzel MC, Delong J, Hawley MC. J Polym Sci A 1995;33:673–89.
[61] Heux L, Halary JL, Lauprêtre F, Monnerie L. Polymer 1997;38: 1767–78.
[62] Heux L, Lauprêtre F, Halary JL, Monnerie L. Polymer 1998;39: 1269–78.
[63] Rubinstein M, Panyukov S. Macromolecules 2002;35:6670–86.
[64] Morgan RJ. Adv Polym Sci 1985;72:1–43.